Fourier domain multispectral multiple scattering low coherence interferometry

Thomas E. Matthews,[1] Michael G. Giacomelli,[2] William J. Brown,[1] and Adam Wax[1,*]

[1]Department of Biomedical Engineering and Fitzpatrick Center for Photonics, Duke University, Durham, North Carolina 27708, USA

[2]Currently with the Research Laboratory of Electronics, Massachusetts Institute of Technology, Cambridge, Massachusetts 02139, USA

*Corresponding author: a.wax@duke.edu

Received 30 September 2013; revised 14 October 2013; accepted 15 October 2013; posted 25 October 2013 (Doc. ID 198350); published 22 November 2013

We have implemented multispectral multiple scattering low coherence interferometry (ms2/LCI) with Fourier domain data collection. The ms2/LCI system is designed to localize features with spectroscopic contrast with millimeter resolution up to 1 cm deep in scattering samples by using photons that have undergone multiple low-angle (forward) scattering events. Fourier domain detection both increases the data acquisition speed of the system and gives access to rich spectroscopic information, compared to the previous single channel, time-domain implementation. Separate delivery and detection angular apertures reduce collection of the diffuse background signal in order to isolate localized spectral features from deeper in scattering samples than would be possible with traditional spectroscopic optical coherence tomography. Light from a supercontinuum source is used to acquire absorption spectra of chromophores in the visible range within a tissue-like scattering phantom. An intensity modulation and digital lock-in detection scheme is implemented to mitigate relative intensity and spectral noise inherent in supercontinuum sources. The technical parameters of the system and comparative analysis are presented.

OCIS codes: (290.0290) Scattering; (100.3175) Interferometric imaging; (290.4210) Multiple scattering.

http://dx.doi.org/10.1364/AO.52.008220

1. Introduction

Tissue scattering limits the penetration depth of most optical imaging techniques by both attenuating the ballistic signal and obscuring it with a diffuse background. Techniques that image with ballistic photons require a way to separate the desired signal from the diffuse background in order to image features in a scattering medium, such as tissue. Confocal microscopy uses a pinhole to accept only light from a given focal plane and reject out-of-focus light; it is effective to about three scattering mean free paths (MFPs), or approximately 200 μm in tissue [1]. Optical coherence tomography (OCT) and other low coherence interferometry (LCI) methods use interferometry to gate backscattered photons by optical path length, thus isolating photons arriving from a specific depth. OCT is sensitive to about 27 scattering MFPs or about 1–2 mm in tissue [2]. Optical penetration depth can be increased by utilizing scattered instead of ballistic light, typically at the cost of reduced resolution. Methods such as diffuse optical tomography utilize scattered light instead of ballistic light to detect features centimeters deep in tissue, with the trade-off of significantly degraded spatial resolution (5–10 mm) [3,4] and the possibility of systematic reconstruction errors [5]. Spatial frequency domain imaging also utilizes scattered light to measure the bulk optical

1559-128X/13/348220-09$15.00/0

properties and thicknesses of layered media [6]. Photoacoustic tomography (PAT) is a powerful method for visualizing absorbers in tissue but offers no scattering-based contrast and requires the imaging device to be in acoustic contact with the sample [7]. More recently, researchers have focused on compensating for tissue turbidity to refocus scattered light [8,9].

Not all scattering media are created equal, and the anisotropy of tissue scattering can be exploited to improve optical imaging capabilities [10]. Multiple scattering low coherence interferometry (ms/LCI) is an imaging technique that uses multiply forward scattered photons to image up to 90 scattering MFPs with millimeter-scale resolution [11]. This corresponds to depths of 5–10 mm in many human tissues [12]. Multiply forward scattered photons are useful in probing tissue because their path much more closely resembles that of ballistic light as opposed to diffusely scattered light. An ms/LCI instrument is capable of imaging more deeply than an OCT instrument of comparable sensitivity because forward scattered photons experience far less attenuation with depth [13]. LCI is an attractive method for the detection and gating of forward scattered photons because it offers both precise determination of time of flight (to a few micrometers) and interferometric gain, which allows shot noise limited detection of a high photon flux.

In this paper we introduce *multispectral* multiply scattered low coherence interferometry in a Fourier domain architecture, which offers two main improvements over the previous time-domain ms/LCI system: multispectral capabilities and significantly faster acquisition times. In addition, the new system incorporates a modulation and digital lock-in detection scheme to overcome the inherent noise problems arising from the use of supercontinuum illumination. Using methods developed for spectroscopic OCT, Fourier domain interferograms acquired in multispectral ms2/LCI can be processed to yield depth-gated reflectance spectra [14,15]. Spectroscopic imaging is desirable because it allows functional as well as structural characterization of a sample. This opens the door to localizing contrast agents and measuring biologically relevant parameters, such as blood vessel oxygenation. Previous time-domain ms/LCI systems sacrificed acquisition speed for the sensitivity necessary to detect the very weak multiply scattered signal [11]. The slow acquisition speed has been a major drawback of ms/LCI. To address this concern, we exploit the sensitivity of Fourier domain LCI, which is independent of both scan depth and spectral bandwidth [16], allowing faster acquisitions and the ability to examine broadband spectroscopic features. Acquisition speed has improved from 1 min per millimeter for the time-domain implementation to 1 min per almost 7 mm A scan for ms2/LCI, a sevenfold improvement in speed. To achieve the high sensitivity (~146 dB) necessary for ms2/LCI, we implemented a modulation and lock-in detection scheme that suppresses the effects of relative intensity and spectral noise common to supercontinuum illumination systems. Using this system, we demonstrate imaging of structural features and acquisition of absorption spectra of chromophores through 90 scattering MFPs.

2. Experimental Design

A. Instrument Layout

A schematic of the ms2/LCI system is shown in Fig. 1(a). The light source was a supercontinuum laser (Fianium SC-450), with the output filtered to remove the unused infrared components >800 nm. A beamsplitting cube (90:10, Thorlabs) generated sample and reference beams for a modified Mach–Zehnder interferometer. Approximately 9 mW of power illuminated the sample. The ~5 mm beam was focused into the sample by a 100 mm focal length lens to a 16 μm beam waist, and the beam was offset from the optical axis of the lens. Backscattered light was collected and collimated by the same lens using an aperture on the opposite side of the optical axis from the illumination beam. The illumination and collection apertures were arranged so that each was at ~4° relative to normal incidence, as shown in Fig. 1(a) (inset). This arrangement serves to reduce the collection of diffusely scattered light, which would otherwise contribute an undesirable background signal [11]. Multiply forward scattered photons from the illumination returned from scattering inhomogeneities in the focal zone (as defined in the figure) within the sample are preferentially detected over diffusely scattered photons [Fig. 1(b)]. Selecting a narrower illumination geometry more parallel to the optic axis (<4°) would have poorer rejection of diffuse photons, while a wider geometry (>4°) would not permit collection of light from the targeted 1 cm depth using this objective lens.

To further increase the sensitivity to deep features, we used the OCT technique of enhanced depth imaging [13], where the zero path delay point of the coherence gate ($z = 0$) is placed behind the focal volume. By placing this region of highest sensitivity deep within the sample, an enhancement is obtained [17]. Cross-sectional images (B scans) of the sample were acquired by laterally translating the sample chamber. The coherent detection scheme had a one-sided depth imaging range of 6.8 mm in air, limited by spectrometer resolution (detailed in the next section). Composite B scans covering depth regions larger than the spectrometer imaging range were created by translating the sample in the axial dimension. A variable delay line with a retroreflector on the reference arm was used to adjust the zero path length point of the interferometric gating between data acquisitions. The light returned from the sample was recombined with the reference beam on another 90:10 beamsplitting cube and coupled into a single mode fiber, which also served as the

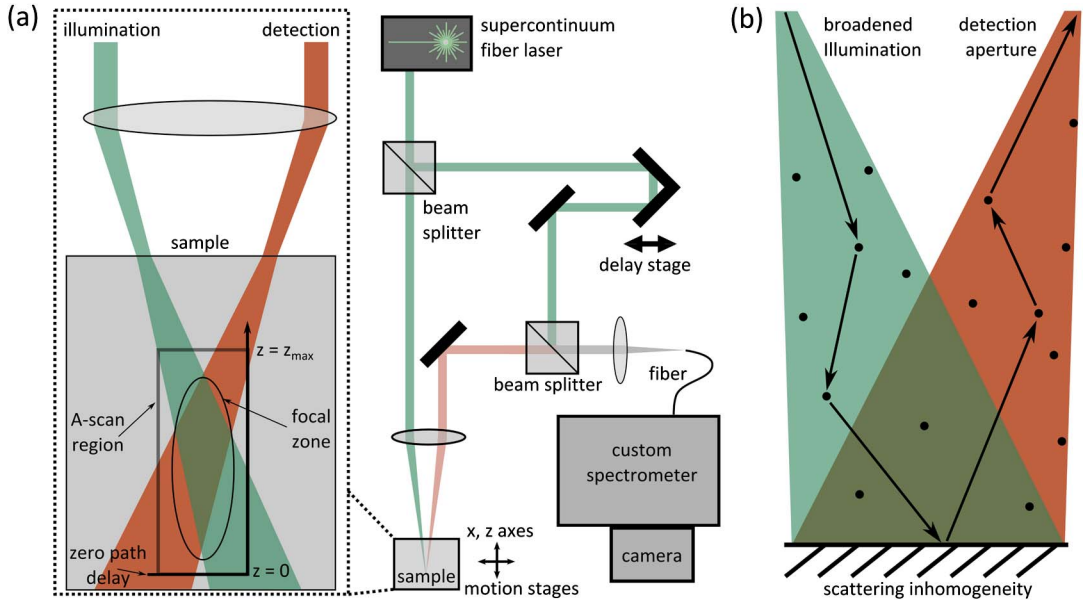

Fig. 1. (a) Diagram of system setup. The ms2/LCI instrument consists of a modified Mach–Zehnder interferometer and a custom spectrometer. The inset shows the arrangement of focal volume in the sample and the location of the zero path delay point. (b) Cartoon illustrating an example path of a multiply forward scattered photon used to image a scattering inhomogeneity.

entrance aperture to the spectrometer. The collection angle of the sample light was limited by the 0.2 mrad diffraction angle of the reference arm.

B. Spectrometer Design and Data Processing

The ms2/LCI instrument has two goals: to measure visible spectroscopic features and to image through many millimeters of sample depth. Fourier domain LCI instruments face a trade-off between imaging range and spectral bandwidth. Imaging range ($z_{\max}$) depends on spectral resolution, and because sensors have a finite array of pixels, a long imaging range requires dispersing the spectrum as much as possible. Highly dispersive spectrometers thus become limited in their spectral bandwidth. (The traditional OCT trade-off of range versus axial spatial resolution is unimportant in this application because multiple scattering creates a distribution of photon path lengths, blurring axial features and removing the need for micron-level axial resolution). We chose to design a highly dispersive spectrometer but use a large sensor array to retain as much spectral bandwidth as possible.

The spectrometer was centered at 633 with 60 nm of bandwidth, with an adjustable center wavelength based on the most relevant spectral features of a sample. A 1800 l/mm grating (Wasatch Photonics) dispersed the collimated output from the fiber, which was then focused onto the camera by a custom objective lens. The sensor was a 12-bit CCD camera (Dalsa Piranha), 4096×96 pixels with a pixel size of 7×7 μm and a maximum line rate of 20 kHz. The vertical direction was fully binned to operate it as a line scan camera. Because the sensor was relatively wide (28 mm), we used an optical design package (Zemax) to optimize the objective lens for a flat focal plane and minimum aberrations at the edge of the camera. Because only the lateral spot size is important to spectral resolution, we optimized to an elliptical spot with an aberration limited lateral size close to the diffraction limit at the expense of a relaxed vertical spot size. The pixel limited spectral resolution was 14.7 pm. The theoretical imaging range ($z_{\max}$) of the LCI system in air was therefore 6.8 mm, which translates to 4.7 mm in our phantom medium after accounting for the increased index of refraction. Based on the measured falloff distance of $z_{6\,\mathrm{dB}} = 2.7$ mm, the actual spot size on the spectrometer sensor was 15.3 μm FWHM [18].

Acquired spectra were individually resampled from wavelength onto an axis linearly spaced in wavenumber (k) by interpolation. Final numerical dispersion compensation was performed on each spectrum, as described previously [19].

C. Sensitivity and Noise in ms2/LCI

In the ms2/LCI spectrometer, the optical power detected by each channel is the sum of three terms [18]:

$$P(k) = P_R(k) + P_s(k) + \sum_n^N 2\sqrt{P_R(k)P_{sn}(k)}\,\cos(k\Delta z_n), \qquad (1)$$

for each wavenumber k, where Δz_n is the location of each reflector n in the sample corresponding to an optical path length difference Δz between the sample and reference interferometer arms. The detected

reference and sample powers for each channel $P_R(k)$ and $P_S(k)$ depend on the product of the illumination source power, the system and spectrometer efficiency, and reference or sample arm reflectivity (R_R or R_S), respectively. The detected reference and sample arm powers are invariant with the location of sample reflectors and do not oscillate with k. Therefore these terms appear at $z = 0$ when the spectral domain signal is Fourier transformed to the spatial domain. The third term is the cross correlation between the sample and reference arm and gives rise to the sample's depth reflectivity profile. Autocorrelation terms proportional to $\sqrt{R_{sm}R_{sn}}\cos(k\Delta z_{smn})$ also exist between features m and n in the sample arm. However, the reflectivity of sample features in practice is very small and their product effectively vanishes. The reference arm signal may also contain autocorrelation terms due to multiple reflections of optical elements, which then contribute undesirable background features.

The signal-to-noise ratio in LCI is defined as the mean squared signal over noise variance: $\mathrm{SNR} = \langle S^2\rangle/\sigma^2_{\mathrm{noise}}$ [16,18,20,21]. Spectral domain LCI detects the real part of the complex spectral density, with the total signal strength $\langle S^2\rangle$ depending on the number of detected photoelectrons during an acquisition of duration Δt:

$$\langle S^2\rangle = (\eta^2\Delta t^2/E_v^2)P_R P_S. \tag{2}$$

Here η is the detector quantum efficiency and E_v is the energy of one photon. The noise variance is the sum of several noise sources, including detector receiver noise, relative intensity noise (σ^2_{RIN}), and shot noise (σ^2_{shot}). Receiver noise is composed of both dark noise and read noise ($\sigma^2_{\mathrm{read}} + \sigma^2_{\mathrm{dark}}$), with read noise usually the dominant term for fast exposures. Read noise is invariant with acquisition parameters and generally depends solely on the camera electronics. The variance of relative intensity noise of a spontaneous, incoherent source scales with source power and bandwidth [21]. This term becomes somewhat more complicated for supercontinuum sources and will be addressed more completely in the next section. Shot noise is white noise originating from the Poisson characteristics of a quantized system and its variance is given (in units of electrons squared per measurement) by [18]

$$\sigma^2_{\mathrm{shot}} = \eta\rho(P_R + P_S)\Delta t/E_v, \tag{3}$$

where ρ is the spectrometer efficiency. In practice, $P_R \gg P_S$, and so only the contribution of reference power to shot noise needs to be considered. With careful instrument design, both read and relative intensity noise can be lowered below the shot noise level, in which case the measurement is described as shot noise limited. In this limit, reference power drops out of the SNR (defined here in units of dB):

$$\langle S^2\rangle/\sigma^2_{\mathrm{shot}} = \eta P_S\Delta t/E_v. \tag{4}$$

Both the interferometric signal strength and shot noise scale with the square root of the reference power. Thus, sensitivity in the shot noise limit solely depends on the number of sample photons detected. Increased sensitivity can be achieved through increased spectrometer efficiency, sample illumination power, or acquisition time. Acquiring signal for longer durations or averaging multiple short acquisitions increases sensitivity by the same amount. Sample illumination power is limited by practical considerations of available light sources and sample damage thresholds. In ms/LCI, the increased sensitivity necessary to measure the extremely low sample flux of multiply scattered photons is achieved by using long acquisition times. Previous time-domain ms/LCI experiments required 1 min per 1 mm of scanned sample depth to gain the desired sensitivity. In this work, we are able to image through similar scattering samples by averaging for 1 min but acquire the entire (~6.8 mm) A scan simultaneously thanks to the advantages of Fourier domain detection, granting an approximately sevenfold speed increase.

We measured the sensitivity of the ms2/LCI system, with a mirror in the sample beam and a calibrated attenuation, to be 97.6 dB for a single spectrum (one line on the camera) with a 125 μs exposure. Instrument losses were estimated at 10.4 dB (70% collection optics efficiency, 50% loss at the polarizing beam splitter, 40% coupling efficiency at the spectrometer input fiber, 80% grating diffraction efficiency, 90% transmission through spectrometer optics, and 90% sensor pixel fill factor), without which sensitivity could be as high as 108.0 dB. The shot noise limited sensitivity was calculated from the maximum sample power (9 mW) to be 120.8 dB [16]. This implies our sensitivity is almost 13 dB lower than the shot noise limit. The increased noise could result from either camera read noise or relative intensity noise. The read noise of our camera was both specified and measured to be well below the shot noise floor. Instead, we hypothesized that relative intensity noise in our supercontinuum light source contributes to the observed SNR degradation. Noise in supercontinuum sources is discussed in more detail below, along with a method for suppressing it.

Previous ms/LCI experiments measured ~140 dB of attenuation of the multiply scattered signal after propagating through 80 scattering MFPs, and ~146 dB attenuation through 95 MFPs in highly anisotropic media ($g > 0.98$) [11]. To detect these signals with the new ms2/LCI instrument, large batches of spectra were acquired, processed to A scans, and incoherently averaged. Incoherent averaging allows for an effective acquisition time much longer than is possible in a single long acquisition due to the limited phase stability of the sample

and maximum well depth of the sensor. To gain the ~50 dB necessary to measure multiply forward scattered photons through 90 scattering MFPs, we averaged up to 1,000,000 spectra (2 min of acquisition) [22]. Note that for an OCT system even with ~140 dB of SNR range, the imaging depth would still only be ~37 scattering MFPs [13].

D. Supercontinuum Noise and Digital Lock-in Detection

For illumination, we chose a supercontinuum laser because it provides a high spectral power density in a single spatial mode. Visible light is needed to see the spectroscopic contrast of interest. Very few single mode sources exist in the visible wavelength spectrum with substantial power and bandwidth.

The pulsed supercontinuum source has its own drawbacks, including relative intensity noise in the supercontinuum output that may be orders of magnitude higher than in the pump laser. Previous work found that the noise in a photonic crystal fiber pumped by a ytterbium-doped fiber laser was higher in the output supercontinuum than in the pump by 30 dB (the same technology used in commercial supercontinuum lasers) [23]. The noise was partially attributed to amplified quantum noise. Other groups showed pulse-to-pulse spectral instabilities greater than 10 dB for individual wavelength components as compared to the mean supercontinuum spectrum [24]. Noise in the supercontinuum output could therefore be responsible for much of the gap between the shot noise limit and our observed sensitivity.

To mitigate the effects of relative intensity and spectral noise in supercontinuum sources, we implemented an intensity modulation and digital lock-in detection scheme. Noise generally has broadband temporal characteristics, and therefore narrowing the detection bandwidth reduces measured noise power. The narrowest detection bandwidth possible is inversely proportional to the measurement time. Shifting detection to higher frequencies and away from zero frequency also moves to regions with lower noise floors, reducing the contribution of $1/f$ noise and any background noise. For intensity modulation, a chopper wheel (Thorlabs MC1000A) was placed in the sample arm. Because the only significant contribution to detected intensity that depends on sample power is the interferometric term [third term in Eq. (1)], noise in the reference spectrum and autocorrelation artifacts will be rejected. (Generally sample power is too low to be directly detected.) To temporally filter the measurement, we first converted every spectrum in each batch acquisition to an A scan. The temporal characteristics for each depth point in the scan were then computed using a fast Fourier transform (FFT). The frequency bin in the FFT corresponding to the known modulation frequency was isolated and rotated by the known phase of the modulation such that the representation of the desired signal that was wholly real was obtained. Only the noise components that overlap in bandwidth and phase with this detection filter will then contribute to the demodulated signal. Thus phase-sensitive demodulation of each batch of acquired data yielded an A scan with reduced noise and background compared to simple bulk averaging. Digital lock-in detection has some advantages over its analog counterpart. First, because it is accomplished in software, there are no limitations to the dynamic range of the measurement. In addition, realization of a digital filter is typically closer to ideal behavior than one might obtain by designing an analog filter.

The scheme was implemented by modulating the sample beam power at 500 Hz using the chopper. A data acquisition (DAQ) board (National Instruments PCIe-6321) generated the driving signal for the chopper, which was stabilized to the reference frequency by a phase-locked loop. The DAQ board also generated a second clock at 16× the chopper frequency that was used to trigger each line acquisition from the spectrometer camera. Due to computer memory constraints, a maximum of 24,576 spectra were acquired in each modulated batch. Acquiring spectra at a rate of 8 kHz gives a total acquisition time of 3.1 seconds per batch, yielding a minimum lock-in detection bandwidth of 0.32 Hz.

E. Spectroscopic Low Coherence Interferometry

Using methods developed for spectroscopic analysis in OCT, we processed acquired interferograms to provide depth-gated spectral reflectivity profiles [14]. We used the short-time Fourier transform (STFT) method, which involves multiplying the acquired spectral interferogram by a series of narrow Gaussian windows at various intervals and calculating the A scan from each windowed spectrum to generate a two-dimensional data set with reflectivity information for both depth and wavenumber, which is termed the time–frequency distribution [25]. We used an STFT window of 1.4 nm, which degrades axial resolution to 130 μm. Much better axial resolution can be achieved using the new dual-window algorithm instead [15]. However, because ms2/LCI not only involves computing a very large number of time–frequency distributions but also has axial resolution inherently degraded by the multiple scattering process [11], there would be little gain from choosing the more computationally intense algorithm here. Individual time–frequency distributions were computed for every acquired spectrum and then incoherently averaged to increase SNR, in the same procedure used for A scans. Because this is a computationally intense but inherently parallel process, we utilized the processing power gains from GPU computing. The nVidia CUDA Fast Fourier Transform library and a commercial graphics card (nVidia GeForce GTS 250) were used for calculation of time–frequency distributions and later for digital lock-in calculations.

F. Samples

Phantoms consisted of a suspension of microspheres (15 μm diameter, polymethyl methacrylate, Bangs

Laboratories) in a neutrally buoyant 70% glycerol/water mix. The scattering liquid filled a glass colorimeter cell (10 mm path length, Fischer Scientific), oriented at a slight angle to avoid the specular reflection from the front of the cell. Scattering properties of the sample were calculated using Mie theory based on the size of the microspheres and the indices of refraction of the microsphere material and glycerol/water mixture. The scattering anisotropy parameter g for these suspensions was calculated to be 0.988. We chose a suspension with a scattering coefficient of 50 cm^{-1} to mimic some human tissues. For example, brain white matter has a reported scattering coefficient of 51 cm^{-1} and an anisotropy parameter g of 0.96 at 633 nm [12]. Targets at the far end of the 1 cm cell were thus imaged through more than 90 scattering MFPs for the combined illumination and detection path length.

3. Results

A. Digital Lock-in Detection of LCI Signal

The results of using the demodulation scheme on the measured noise and background in an ms2/LCI experiment are shown in Fig. 2(a). The solid trace shows the A scan of a highly attenuated signal from a mirror (white arrow) obtained by averaging one batch of 24,576 spectra. Note both the imperfectly subtracted zero frequency artifact and the spurious autocorrelation signal highlighted by the solid arrows. Imperfect subtraction of these artifacts results from drift in the reference spectrum. The improvement in SNR can be seen by comparing the solid trace to the demodulated scan shown by the dashed trace, which was calculated from the same batch acquisition. The A scans have been normalized at the mirror peak and slightly offset laterally for clarity. The traces have not been offset vertically; the solid trace calculated without demodulation contains a significant background that limits SNR. We found lock-in detection typically increases SNR between 5 and 10 dB, depending on which region of the A scan was examined. The noise floor was seen to increase toward lower frequency spectral components, which we attribute to the structure of the source spectrum. In addition, modulation is very effective at suppressing the zero frequency artifact and autocorrelation features.

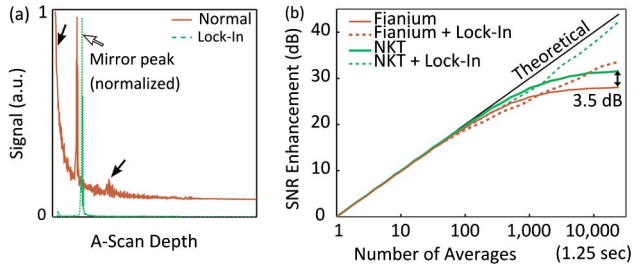

Fig. 2. (a) Reduction of noise, background, and artifacts in an A scan by implementing digital lock-in detection. Solid arrows highlight the zero frequency and autocorrelation artifacts. Scans have been slightly offset laterally for clarity. (b) Relative SNR enhancements measured by averaging increasingly larger numbers of scans. Enhancements near the theoretical prediction occur up to about 1,000 averages, after which noise in the background signal limits further improvement. The NKT source was found to have a lower background signal than the Fianium. Lock-in detection reduced the effect of the background, allowing further gains by averaging larger numbers of spectra. With lock-in detection, the NKT was ~8.7 dB more sensitive than the Fianium when analyzing a full batch of 24,576 spectra.

Characterization of this system shows that raw averaging is only effective at reducing noise to a point. After 1,000 acquisitions there was diminished SNR enhancement from averaging [Fig. 2(b)]. Averaging for 3 s provided an SNR enhancement 15.9 dB lower than the theoretically predicted enhancement. This phenomenon results from a static or semi-static background signal being revealed as the noise floor is lowered. This background was found to be present in the highly structured nature of the supercontinuum spectrum, which has components at least as fine as 0.02 nm. These findings are similar to those of other groups [24]. Instabilities in the fine structures mean they cannot be easily subtracted off as a background signal. These slowly drifting components cannot be easily averaged away because they vary on a time scale similar to the averaged measurement. Examination of the structured background showed it evolved only partially on a scale of minutes. As SNR improves during averaging, the relative contribution to the noise floor from this structured background increases, creating the SNR ceiling shown in Fig. 2(b). Digital lock-in detection was effective at removing the background, allowing for larger SNR enhancements with highly averaged acquisitions.

B. Comparison of Different Supercontinuum Sources

Because supercontinuum properties depend on a number of instrument parameters, we sought to compare the noise characteristics of different supercontinuum sources to fully characterize the enhancements that are obtained with the demodulation scheme. Supercontinuum generation is a highly nonlinear process that depends on pump laser characteristics, pulse duration, photonic crystal fiber length, nonlinearity, zero dispersion wavelength, and so forth. Sources from different manufacturers are likely to differ. We compared the Fianium SC-450 with the NKT SuperK Extreme ZXW-12 to empirically determine how the source affects noise and background levels and how the demodulation scheme can mitigate its effect. We acquired batch spectra from each source at identical power levels in our spectral window. The Fianium was found to have a larger noise floor [~3.5 dB, Fig. 2(b)] due to fluctuating fine spectral features. The lock-in detection scheme was more effective at approaching the theoretical SNR enhancement for long averages with the NKT source. However, because our access to the NKT source was limited, the Fianium was used for the rest of the experiments reported here.

C. Characteristics of ms2/LCI Imaging

We wished to determine how multiple scattering affected lateral and axial resolutions in the ms2/LCI system. A narrow imaging target was placed in a scattering suspension (50 cm^{-1}). The target was a flat capillary tube with a gold coating on its front face, to act as a scattering inhomogeneity. B-scan images were acquired with the target located at various depths (3.0 mm, 6.1 mm, and 8.6 mm), which corresponded to imaging through 27, 55, and 77 scattering MFPs, respectively. A diagram of the sample geometry is shown in Fig. 3(a), followed by ms2/LCI B scans of the target. It can be seen that multiple scattering broadens the image of the target both laterally and axially, which is expected from previous measurements [11,13]. Depth-summed lateral profiles of the target at the various depths are shown in Fig. 3(b). The lateral and axial resolution of the system was determined from the 10% to 90% rise in the signal from the target [Figs. 3(c) and 3(d)]. It can be seen that lateral resolution is rapidly degraded until it reaches a maximum at 55 MFP. After this point, light that is further deflected is completely ejected from the detection cone and does not contribute to the ms2/LCI signal such that further degradation is not seen. Conversely, axial resolution becomes steadily coarser with an increasing number of scattering events, until the signal is too degraded to measure.

D. Spectroscopic Contrast

A key feature of the ms2/LCI system is its ability to measure depth-gated spectral reflectivity profiles. To demonstrate this, we constructed another phantom with spectroscopic features. A mirrored coverslip was placed in the back of the sample chamber. In front was placed a rectangular capillary filled with green food coloring [Fig. 4(a)]. The depth was such that the mirror was imaged through 90 scattering MFPs, near the limit of our system and more than 2 times the limit of conventional OCT [2]. Depth-gated reflectance spectra were extracted from the acquired interferograms with the STFT method. The reflectance spectra were binned into three spectral windows, which were weighted as red, green, and blue images and combined to give a false color B scan of the sample, which provides the ability to highlight spectroscopic features [Fig. 4(b)]. White balance was set based on the reflectivity of the mirrored coverslip. The capillary is in the indicated region of interest (ROI). Because the dye preferentially absorbed light below 650 nm, its shadow appears red in the reflectance image, even though the capillary itself is not seen in this image. The reflectance spectrum from behind the dye-filled capillary was converted to an absorption spectrum, as shown in Fig. 4(c). The measured absorption spectrum closely matched the reference spectrum of the dye measured with a conventional spectrometer (HR-4000, Ocean Optics).

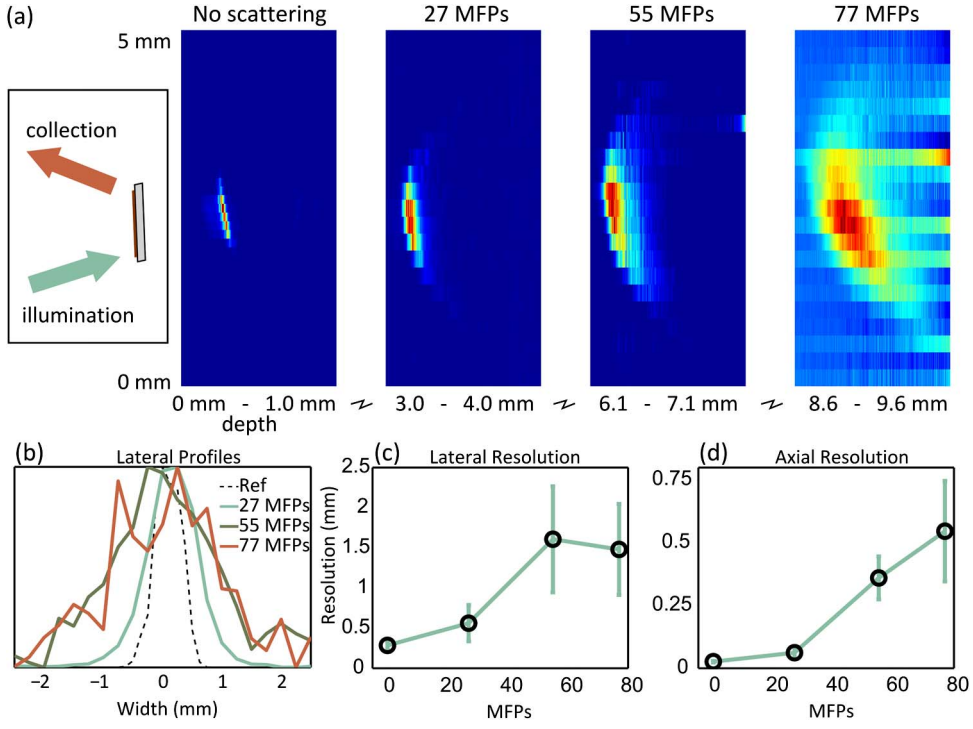

Fig. 3. (a) Sample geometry of the resolution target and B scans through no scattering medium and at increasing depths in a 50 cm^{-1} bead suspension. The total number of scattering MFPs is indicated at the top of each image, and the physical depth at the base. Multiple scattering broadens the image of the target both laterally and axially. (b) Lateral profiles of the target at various depths. (c) Lateral and (d) axial resolution measured at various depths, calculated from the 10% to 90% signal rise, and error bars based on the standard deviation of the measurement. Lateral resolution broadening apparently saturates after 55 MFPs, but axial resolution broadening continues.

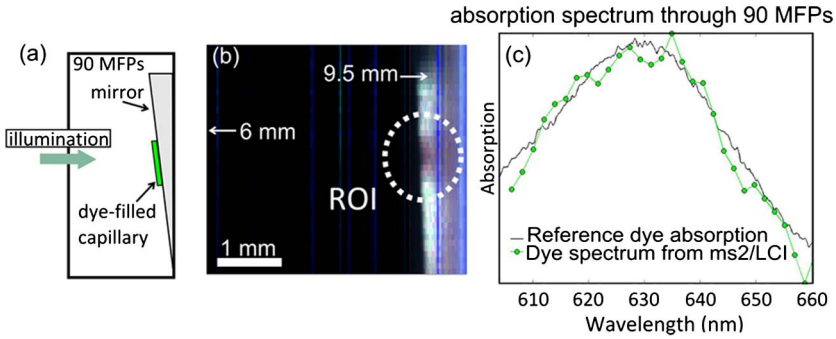

Fig. 4. (a) Cartoon showing spectroscopic sample geometry, with a mirror and dye-filled capillary imaged through 90 MFPs. The mirror is placed at a slight angle to the sample chamber to avoid the specular reflection from the front of the chamber. (b) False-colored B scan of the sample based on the depth-gated spectral reflectivity profiles. The ROI signal is red because the dye superficial to this region preferentially absorbs light below 650 nm. (c) Calculated absorption spectrum of the ms2/LCI signal of the ROI compared to a reference spectrum for the dye, showing good agreement.

4. Discussion

We have shown ms2/LCI as a viable method for acquiring images with spectroscopic contrast and millimeter-scale resolution in thick tissue-like samples. It is important to note, however, the ways in which the ms2/LCI images deviate from ideal representations of the sample. Imaged objects are shifted to deeper positions from their true depth, because multiply scattered light accumulates extra travel time. This axial shift needs to be considered when interpreting ms2/LCI imaging data. Unlike the micrometer axial resolution of OCT, here the resolution is on the order of 1–2 mm. Even though interferometric gating can bin photon path length with micrometer precision, multiple scattering events create a distribution of path lengths for photons scattered by an object of interest. The millimeter-scale resolution achieved here is in a mesoscopic regime between typical interferometric methods (OCT) and diffuse imaging techniques. It is important to note that the strength of the ms2/LCI signal depends on the magnitude of the scattering inhomogeneity to be imaged. In these experiments we used test targets that reflected all incident light. Biological samples will return less light and therefore require longer imaging times or shallower scans. This method is also very dependent on both the scattering coefficient of a given tissue type and its anisotropy parameter. Lower degrees of anisotropy, such as that in skin tissue, will decrease scan depth.

We also note the ms2/LCI method does not yield the ideal reflectance spectrum of the sample at each depth. Rather, similarly to spectroscopic OCT it gives the spectrum of light being returned from each depth in the sample. Light returning from deep in the sample will have experienced absorptive and scattering losses from each layer above and so carries information about both shallow features and deep features. Careful interpretation of the data is necessary in order to conduct quantitative spectroscopic analysis. Scattering is a wavelength-dependent process and will have an effect on the measured reflectance from various depths. Finally, to detect spectroscopic features in a sample, a scattering inhomogeneity is necessary to return light back to the surface after it has sampled the spectroscopic feature of interest.

The use of a supercontinuum source in the ms2/LCI scheme presents unique considerations for system development. Supercontinuum sources have attracted increased interest in the last few years, because of their high spectral power density and extreme bandwidth. They also introduce new problems related to intensity noise and spectral noise. Our digital lock-in detection method mitigates many of these drawbacks and provides similar advantages to balanced detection. Balanced detection, which is often used in time-domain or swept source LCI systems, is difficult to implement in spectral domain systems [26]. Digital lock-in detection provides a simple alternative that enables significant gains in SNR.

The ms2/LCI method has the potential to fill a gap in mesoscopic tissue imaging applications. Multiple low-angle scattered photons can probe several times more deeply than ballistic methods (depending on the anisotropy of the medium). There are also several advantages over diffuse tomography and spectroscopy methods. For example, spatial frequency domain imaging has found success imaging absorptive and scattering objects in turbid media but has not done so at a depth of 10 mm in tissue-like media [6]. Both time-resolved and frequency domain diffuse optical tomography employ temporal gating to select photons with a path length close to ballistic propagation and therefore reduce the probed volume [27,28]. As typically implemented, electronic gating or frequency domain systems substantially limit temporal resolution, reducing the ability to select ballistic paths. Better time resolution can be achieved using streak cameras and time-correlated single photon counting, but these have very low optical throughput, resulting in lower imaging speed and signal strength. Temporal gating schemes typically restrict measurements to just a few individual wavelengths, restricting their ability to provide spectroscopic information. The advantages of ms2/LCI include high throughput with superior temporal gating and full

spectral information across the illumination bandwidth. While the instrument presented here offers many improvements, acquisition speed remains as the largest hurdle in implementing clinically useful ms2/LCI systems.

Another imaging modality designed to work deep in scattering samples with absorption-based contrast is PAT. PAT has strengths and weaknesses compared to ms2/LCI. PAT retains excellent resolution many centimeters into tissue (with resolution approximately 1/200th of imaging depth) [7]. Absorption of excitation light is imaged by ultrasound detectors. However, there are two drawbacks that make PAT unsuitable for many applications. Because it relies on ultrasound detection, the imaging device must be in acoustic contact with the sample, typically achieved with ultrasound gel or by immersing the sample in a water tank. While ms2/LCI offers spectroscopic contrast as an added enhancement, PAT requires the presence of an absorber. Structural features and scattering inhomogeneities can be imaged by ms2/LCI. Finally, ms2/LCI offers full spectral measurements across its illumination bandwidth in a single image, while PAT requires wavelength shifting and reimaging to build up images based on more than one wavelength.

In conclusion, we have demonstrated acquisition of depth-gated spectroscopic information from the ms2/LCI measurement through 90 MFPs of tissue-mimicking phantoms with improved acquisition speeds compared to previous systems. This opens new avenues in the field of multispectral imaging with scattered photons.

We gratefully acknowledge funding support from the National Science Foundation (CBET 1133222). We would also like to thank Yuankai Tao for his helpful discussions.

References

1. C. L. Smithpeter, A. K. Dunn, A. J. Welch, and R. Richards-Kortum, "Penetration depth limits of in vivo confocal reflectance imaging," Appl. Opt. **37**, 2749–2754 (1998).
2. M. R. Hee, J. A. Izatt, J. M. Jacobson, J. G. Fujimoto, and E. A. Swanson, "Femtosecond transillumination optical coherence tomography," Opt. Lett. **18**, 950–952 (1993).
3. T. Durduran, R. Choe, W. B. Baker, and A. G. Yodh, "Diffuse optics for tissue monitoring and tomography," Rept. Progr. Phys. **73**, 076701 (2010).
4. J. A. Moon, R. Mahon, M. D. Duncan, and J. Reintjes, "Resolution limits for imaging through turbid media with diffuse light," Opt. Lett. **18**, 1591–1593 (1993).
5. X. Cheng and D. Boas, "Systematic diffuse optical image errors resulting from uncertainty in the background optical properties," Opt. Express **4**, 299–307 (1999).
6. D. J. Cuccia, F. Bevilacqua, A. J. Durkin, and B. J. Tromberg, "Modulated imaging: quantitative analysis and tomography of turbid media in the spatial-frequency domain," Opt. Lett. **30**, 1354–1356 (2005).
7. L. V. Wang and S. Hu, "Photoacoustic tomography: in vivo imaging from organelles to organs," Science **335**, 1458–1462 (2012).
8. X. Xu, H. Liu, and L. V. Wang, "Time-reversed ultrasonically encoded optical focusing into scattering media," Nat. Photonics **5**, 154–157 (2011).
9. B. Judkewitz, Y. M. Wang, R. Horstmeyer, A. Mathy, and C. Yang, "Speckle-scale focusing in the diffusive regime with time reversal of variance-encoded light (TROVE)," Nat. Photonics **7**, 300–305 (2013).
10. Y. Choi, T. D. Yang, C. Fang-Yen, P. Kang, K. J. Lee, R. R. Dasari, M. S. Feld, and W. Choi, "Overcoming the diffraction limit using multiple light scattering in a highly disordered medium," Phys. Rev. Lett. **107**, 023902 (2011).
11. M. G. Giacomelli and A. Wax, "Imaging beyond the ballistic limit in coherence imaging using multiply scattered light," Opt. Express **19**, 4268–4279 (2011).
12. W. F. Cheong, S. A. Prahl, and A. J. Welch, "A review of the optical properties of biological tissues," IEEE J. Quantum Electron. **26**, 2166–2185 (1990).
13. M. G. Giacomelli and A. Wax, "Imaging contrast and resolution in multiply scattered low coherence interferometry," IEEE J. Sel. Top. Quantum Electron. **18**, 1050–1058 (2012).
14. U. Morgner, W. Drexler, F. X. Kärtner, X. D. Li, C. Pitris, E. P. Ippen, and J. G. Fujimoto, "Spectroscopic optical coherence tomography," Opt. Lett. **25**, 111–113 (2000).
15. F. Robles, R. N. Graf, and A. Wax, "Dual window method for processing spectroscopic optical coherence tomography signals with simultaneously high spectral and temporal resolution," Opt. Express **17**, 6799–6812 (2009).
16. M. Choma, M. Sarunic, C. Yang, and J. Izatt, "Sensitivity advantage of swept source and Fourier domain optical coherence tomography," Opt. Express **11**, 2183–2192 (2003).
17. R. F. Spaide, H. Koizumi, and M. C. Pozonni, "Enhanced depth imaging spectral-domain optical coherence tomography," American J. Ophthalmol. **146**, 496–500 (2008).
18. R. Leitgeb, C. Hitzenberger, and A. Fercher, "Performance of Fourier domain vs. time domain optical coherence tomography," Opt. Express **11**, 889–894 (2003).
19. Y. Zhu, N. G. Terry, J. T. Woosley, N. J. Shaheen, and A. Wax, "Design and validation of an angle-resolved low-coherence interferometry fiber probe for in vivo clinical measurements of depth-resolved nuclear morphology," J. Biomed. Opt. **16**, 011003 (2011).
20. A. M. Rollins and J. A. Izatt, "Optimal interferometer designs for optical coherence tomography," Opt. Lett. **24**, 1484–1486 (1999).
21. J. F. de Boer, B. Cense, B. H. Park, M. C. Pierce, G. J. Tearney, and B. E. Bouma, "Improved signal-to-noise ratio in spectral-domain compared with time-domain optical coherence tomography," Opt. Lett. **28**, 2067–2069 (2003).
22. N. Nassif, B. Cense, B. Hyle Park, S. H. Yun, T. C. Chen, B. E. Bouma, G. J. Tearney, and J. F. de Boer, "In vivo human retinal imaging by ultrahigh-speed spectral domain optical coherence tomography," Opt. Lett. **29**, 480–482 (2004).
23. U. Møller, S. T. Sørensen, C. Jakobsen, J. Johansen, P. M. Moselund, C. L. Thomsen, and O. Bang, "Power dependence of supercontinuum noise in uniform and tapered PCFs," Opt. Express **20**, 2851–2857 (2012).
24. B. Wetzel, A. Stefani, L. Larger, P. A. Lacourt, J. M. Merolla, T. Sylvestre, A. Kudlinski, A. Mussot, G. Genty, F. Dias, and J. M. Dudley, "Real-time full bandwidth measurement of spectral noise in supercontinuum generation," Scientific Reports **2**, 882 (2012).
25. R. N. Graf and A. Wax, "Temporal coherence and time-frequency distributions in spectroscopic optical coherence tomography," J. Opt. Soc. Am. A **24**, 2186–2195 (2007).
26. W.-C. Kuo, C.-M. Lai, Y.-S. Huang, C.-Y. Chang, and Y.-M. Kuo, "Balanced detection for spectral domain optical coherence tomography," Opt. Express **21**, 19280–19291 (2013).
27. M. S. Patterson, B. Chance, and B. C. Wilson, "Time resolved reflectance and transmittance for the noninvasive measurement of tissue optical properties," Appl. Opt. **28**, 2331–2336 (1989).
28. B. Pogue, M. Testorf, T. McBride, U. Osterberg, and K. Paulsen, "Instrumentation and design of a frequency-domain diffuse optical tomography imager for breast cancer detection," Opt. Express **1**, 391–403 (1997).